

Modeling pressure effects on the turbulent burning velocity for lean hydrogen/air premixed combustion

Zhen Lu^{a,b}, Yue Yang^{a,b,c}

^a*State Key Laboratory for Turbulent and Complex Systems, College of Engineering, Peking University, Beijing 100871, China*

^b*BIC-ESAT, Peking University, Beijing 100871, China*

^c*CAPT, College of Engineering, Peking University, Beijing 100871, China*

Abstract

We investigate and model pressure effects on the turbulent burning velocity over a wide range of pressures and turbulence intensities with the direct numerical simulation (DNS) of statistically planar turbulent premixed flames for lean hydrogen/air mixture. DNS results indicate that the stretch factor has an impact on the turbulent burning velocity and flame surface area at elevated pressures. In particular, the enhanced stretch factor at high pressures increases the ratio of turbulent and laminar burning velocities, diminishing the “bending” effect. Based on a good consistency between turbulent and laminar burning velocities with respect to flame stretch, a lookup table formed by laminar flame data is employed to model the stretch factor in turbulent flames at various pressures. A predictive model for the turbulent burning velocity is then developed by combining sub models of the stretch factor and flame surface area. The overall good agreement between model predictions and DNS results demonstrates that the proposed model is able

*Corresponding author:

Email address: `yyg@pku.edu.cn` (Yue Yang)

to quantitatively predict the turbulent burning velocity over a wide range of pressures and turbulent intensities in homogeneous isotropic turbulence.

Keywords:

turbulent burning velocity, elevated pressure, turbulent premixed flame, direct numerical simulation

1. Introduction

The turbulent burning velocity s_T is one of the most important quantities characterizing turbulent premixed combustion [1–3]. Extensive efforts have been made to investigate the dependence of s_T on various factors such as the fuel composition and chemistry, turbulence intensity, and pressure.

Considering engine relevant conditions, the pressure influence on s_T has been widely reported in experimental works [4–10]. Most studies noticed that the laminar burning velocity s_L^0 of unstretched flames decreases with pressure, whereas s_T is insensitive to or even increased with pressure [7], so the ratio s_T/s_L^0 rises with pressure. Another important observation is the suppression of the “bending” effect [2] of s_T/s_L^0 at elevated pressures [4, 5]. These phenomena have been attributed to small-scale wrinkling of turbulent flame surfaces [5, 11]. Various power laws and scaling methods [7, 10] have been proposed to collapse s_T curves with respect to pressure, but the pressure effects on s_T has not been clearly elucidated and quantitatively modeled.

The direct numerical simulation (DNS) is useful to interrogate detailed information of turbulent combustion [12]. Eulerian [13, 14] and Lagrangian [15] investigations have been employed to explain interactions between turbulence and local flame speed, and to develop correlations between flame

stretch and s_T [16]. The bending curve has been reproduced by DNS [17, 18] at 1 atm, confirming it is caused by the inhibited growth of flame areas.

In recent years, three-dimensional DNS of turbulent premixed flames at elevated pressures were reported by several groups for practical interest [19–22]. Savard *et al.* [19] studied pressure effects on complex fuels in engine relevant conditions. By comparing turbulent flame statistics at 1 and 20 atm with the same Karlovitz number, they argued that the flame area, rather than the stretch factor, causes differences in s_T for iso-octane. Wang *et al.* [20] reported a series of DNS of lean methane/air turbulent flames with various turbulence intensities at 20 atm, and also found that the flame area is the dominant factor for s_T . By contrast, some experimental studies [7, 23] indicated that the stretch sensitivity could be crucial for mixtures with negative Markstein numbers.

A predictive model of s_T is of practical interest for industrial design and combustion modeling [1, 24]. A number of empirical models have been proposed for s_T [2, 3]. However, most of them are not validated over the wide range of pressures and turbulence intensities, and the various power-law scalings strongly depend on empirical parameters [2, 3]. Recently, You and Yang [18] proposed a s_T model based on Lagrangian statistics of propagating surfaces [25, 26]. By estimating the flame area with universal model constants obtained from homogeneous isotropic turbulence (HIT), the model successfully predicts s_T/s_L^0 for various fuels at 1 atm, but the constant s_L^0 used in the modeled area growth rate of flames limits its application to standard pressure.

In this work, we carry out a systematic DNS study of lean H₂/air turbu-

lent premixed flames at a wide range of pressures and turbulence intensities. Statistics of s_T and flame surface areas are investigated to gain insight of underlying governing processes for the bending of s_T . Effects of the flame stretch on local flame propagation in turbulent flames are then analyzed thoroughly over the wide range of parameters. According to the analysis, we propose a new model for predicting s_T , considering variations of both the stretch factor and flame area with respect to pressure. Finally, the model is validated by DNS results.

2. Simulation overview

2.1. DNS parameters

For the DNS of turbulent premixed flames, we consider the free propagation of a statistical planar premixed flame along the streamwise direction in statistically stationary HIT at a range of pressures $p = 1, 2, 5, 10$ atm. The unburnt gas is a lean hydrogen/air mixture with the equivalence ratio 0.6 at the temperature $T_u = 300$ K. For each pressure, the thermal thickness $\delta_L^0 = (T_b - T_u)/|\nabla T|_{\max}$, the laminar flame speed s_L^0 , the displacement speed s_d^0 at the temperature T_{peak}^F corresponding to the peak fuel consumption rate obtained in the freely propagating laminar flame, and the flame Reynolds number $\text{Re}_F = s_L^0 \delta_L^0 / \nu$ with the kinematic viscosity ν are listed in Table 1, where T_b is the temperature of the burnt gas, $|\nabla T|_{\max}$ denotes the maximum temperature gradient in the laminar flame, and the superscript 0 denotes a quantity in unstretched flames.

For each pressure, we conduct four DNS cases with a range of turbulence intensities $u'/s_L^0 = 2, 5, 10, \text{ and } 20$ (i.e., in total of 16 DNS cases in the present

Table 1: Parameters of unstretched laminar flames

p (atm)	1	2	5	10
δ_L^0 (μm)	365.4	178.8	83.16	58.40
s_L^0 (m/s)	0.833	0.646	0.410	0.240
s_d^0 (m/s)	3.22	2.66	1.81	1.12
$T_{\text{peak}}^{\text{F}}$ (K)	1294.0	1366.4	1471.3	1569.2
Re_{F}	15.7	11.9	8.77	7.23

study). The parameters for combustion DNS are listed in Table 2, where u' is the rms velocity fluctuation, and the ratio between turbulence integral scale l_t and flame thickness δ_L^0 is kept as unity. Dimensionless numbers are listed in Table 2. The Damköhler number $\text{Da} = \tau_e/\tau_f = (l_t/\delta_L^0)(s_L^0/u')$ is defined as the ratio of the integral timescale τ_e and the flame timescale τ_f . The Karlovitz number $\text{Ka} = (u'/s_L^0)^{\frac{3}{2}}(\delta_L^0/l_t)^{\frac{1}{2}}$ is defined with the dissipation rate [14]. The turbulence Reynolds number $\text{Re} = \text{Re}_0\text{Re}_{\text{F}}$ is linked with $\text{Re}_0 = (u'/s_L^0)(l_t/\delta_L^0)$ in the regime diagram. We remark that the definitions of Da , Ka , and Re_0 are independent of pressure, so the DNS cases with the same u'/s_L^0 but at different pressures are at the same point in the regime diagram [1].

2.2. Numerical methods

The present DNS solves the low Mach number, variable density formulation of transport equations for mass, momentum, species, and temperature using the NGA code [27], with the Strang splitting applied for transport–chemistry coupling [28]. For the transport part, equations are advanced by

Table 2: Parameters of turbulent combustion DNS

u'/s_L^0	2	5	10	20
l_t/δ_L^0	1	1	1	1
Re_0	2	5	10	20
Da	0.5	0.2	0.1	0.05
Ka	2.828	11.18	31.62	89.44

an iterative semi-implicit Crank–Nicolson scheme [29]. A second-order centered, kinetic-energy conservative finite difference scheme is used for discretizing spatial derivatives in momentum equations, and a third-order bounded QUICK scheme [30] is used for treating convection terms in scalar transport equations of species mass fractions and temperature. The time integration of chemical substep is performed by the stiff solver DVODE [31]. The detailed nine-species H_2/air mechanism [32] is employed, and molecular transport is modeled with constant Lewis numbers for each species [33]. Each DNS case is first run for at least $10\tau_e$ to reach a statistically stationary state, and then statistics are calculated over a period of at least $15\tau_e$.

The computational domain is a cuboid with sides $L_x \times L_y \times L_z = 12L \times L \times L$ and $L = 5.3l_t$. This domain is discretized on uniform grid points $N_x \times N_y \times N_z = 12N \times N \times N$. The numerical resolution in all the cases is ensured to resolve the smallest turbulent and flame length scales by the criterion $k_{\max}\eta \geq 1.5$ [34] and a minimum of 24 grid points within a flame thickness δ_L^0 , respectively, where $k_{\max} = \pi N/L$ is the maximum wavenumber magnitude in DNS of HIT and η is the Kolmogorov length scale. To meet the criteria, we set $N = 128$ for all the cases listed in Table 2 except $N = 256$ for

the case with $u'/s_L^0 = 20$ and $p = 1$ atm. The timestep is controlled by the CFL number less than 0.5. The computational domain has inflow and outflow conditions in the streamwise x -direction, and periodic boundary conditions are imposed in lateral y - and z -directions. The inflow is generated by a separate DNS of non-reacting, statistically stationary HIT, and it is imposed on the bulk inflow velocity in the x -direction. The flame is initialized by the unstretched laminar flame solution, with the flame front laid in the middle of the x -direction. A stable, linear velocity forcing [35] is adopted to maintain the turbulent intensity from $x = 0.5L$ to $9L$ along the streamwise direction. The setup and accuracy of the DNS solver have been validated in Ref. [18].

3. Results and discussions

3.1. Turbulent burning velocity and flame area

We define the turbulent burning velocity by the consumption speed

$$s_T = \frac{1}{\rho_u Y_{F,u} A_L (t_2 - t_1)} \int_{t_1}^{t_2} \int_{\Omega} -\dot{\omega}_F dV dt \quad (1)$$

where the subscript u is for unburnt conditions, $A_L = L_y \times L_z$ is the laminar flame area, $t_2 - t_1$ is the period for collecting statistics, $\dot{\omega}_F$ is the fuel consumption rate, and Ω denotes the entire computational domain. The turbulent flame area A_T is evaluated at the isothermal surface of $T = T_{\text{peak}}^F$ via the marching cubes algorithm.

Figure 1 plots ratios of burning velocities and flame areas against u'/s_L^0 for different pressures. We observe the bending of s_T/s_L^0 for a range of pressures. Meanwhile, the starting point of the bending occurs at larger u'/s_L^0 with the increase of pressure, from $u'/s_L^0 \approx 5$ for $p = 1$ atm to $u'/s_L^0 \approx 10$ for

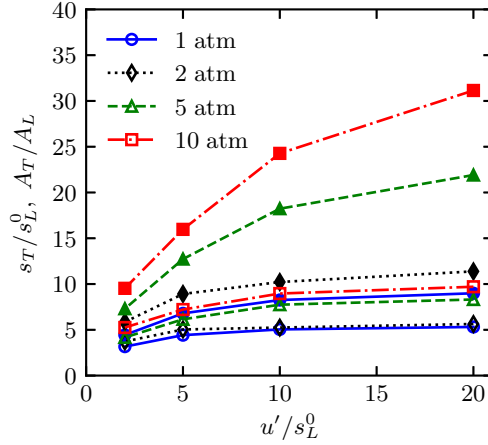


Figure 1: Normalized turbulent burning velocities (solid symbols) and flame areas (open symbols) at a range of pressures and turbulence intensities.

$p = 10$ atm. The diminished bending effect at elevated pressures was also reported in experiments for various fuels [4, 5, 7]. On the other hand, the bending of A_T/A_L appears to be consistent at different pressures. Thus the turbulent burning velocity is significantly accelerated at high pressures, e.g., s_T/s_L^0 at 10 atm is about four times of that at 1 atm in the present flame with $u'/s_L^0 = 20$. By contrast, the variation of A_T/A_L with the pressure is much less than that of s_T/s_L^0 , e.g., A_T/A_L at 10 atm is less than two times of that at 1 atm for $u'/s_L^0 = 20$.

Figure 2 depicts temperature contours at various pressures and $u'/s_L^0 = 10$, and flame shapes appear to be similar. We also find that distributions of the normalized mean curvature of flames are self-similar at different pressures (not shown), as reported in previous studies [19, 21]. Additionally, the temperature around the flame front at 10 atm is much higher than that at 1 atm.

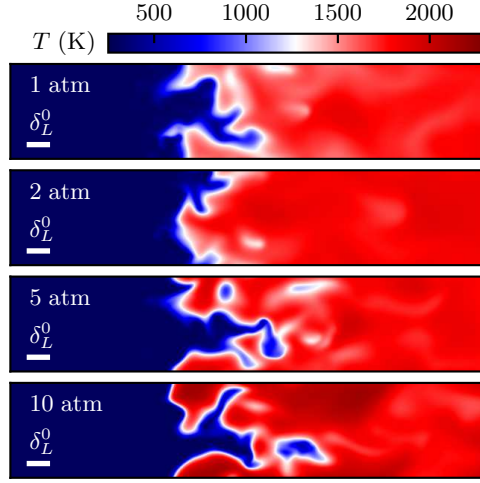


Figure 2: Temperature contours of the turbulent premixed flames at $u'/s_L^0 = 10$ and various pressures.

The Damkhöler assumption $s_T/s_L \sim A_T/A_L$ implies that the growth of s_T is primarily due to the enhancement of A_T by straining motions in low-intensity turbulence. The underlying assumption is that s_L remains valid for the local propagation speed of flame fronts, and typically is taken as s_L^0 of unstretched laminar flames. With the consumption-based definition [3], the two ratios are linked by the stretch factor $I_0 = \langle s_L \rangle / s_L^0$ [36] as

$$\frac{s_T}{s_L^0} = I_0 \frac{A_T}{A_L}, \quad (2)$$

where $\langle \cdot \rangle$ denotes the average over the turbulent flame front. This expression distinguishes contributions to s_T into the area ratio from turbulence effects and the stretch factor due to the flame response under flow variations. Therefore, Eq. (2) and the different bending trends of s_T/s_L^0 and A_T/A_L in Fig. 1 suggest that I_0 should depend on both turbulent intensity and pressure.

3.2. Stretch factor

The stretch factor is close to unity at standard pressure, but it can vary at elevated pressures. Thus we study the effects of turbulence intensity and pressure on I_0 in detail, along with the investigation on flame stretching and its influence on local flame speed.

The stretch factor

$$I_0 = \frac{\langle s_L \rangle}{s_L^0} \approx \frac{\langle s_d \rangle}{s_d^0} \quad (3)$$

is estimated using the local displacement speed [15]

$$s_d = \frac{\nabla \cdot (\lambda T) - \sum_{i=1}^{n_s} c_{p,i} \mathbf{j}_i \cdot \nabla T + c_p \dot{\omega}_T}{\rho c_p |\nabla T|} \quad (4)$$

calculated on the isothermal surface of $T = T_{\text{peak}}^F$, where λ is the thermal conductivity, c_p and $c_{p,i}$ are respectively heat capacities of mixture and species i , \mathbf{j}_i is the diffusion flux of species i , n_s is the number of species, and $\dot{\omega}_T$ is the thermal production term. Then Eq. (2) is approximated by

$$\frac{s_T}{s_L^0} \approx \frac{\langle s_d \rangle}{s_d^0} \frac{A_T}{A_L}. \quad (5)$$

To compare different stretch effects, the stretch Karlovitz number $\text{Ka}_S = \text{Ka}_T + \text{Ka}_C$ is decomposed into $\text{Ka}_T = (\delta_L^0/s_d^0)a_t$ for tangential straining and $\text{Ka}_C = (\delta_L^0/s_d^0)s_d\kappa$ for curvature stretch [16], where $a_t = \nabla \cdot \mathbf{u} - \mathbf{nn} : \nabla \mathbf{u}$ is the tangential strain rate, and $\kappa = \nabla \cdot \mathbf{n}$ is the mean curvature with the surface normal $\mathbf{n} = -\nabla T/|\nabla T|$. All these quantities are first calculated in Ω and then interpolated to the flame surface [13].

Figure 3 compares probability density functions (PDFs) of Ka_S , Ka_T , Ka_C , and s_d/s_d^0 between pressures 1 atm and 10 atm with $u'/s_L^0 = 2$ and 10. We observe that PDFs of both Ka_S and Ka_T in all the cases exhibit positive

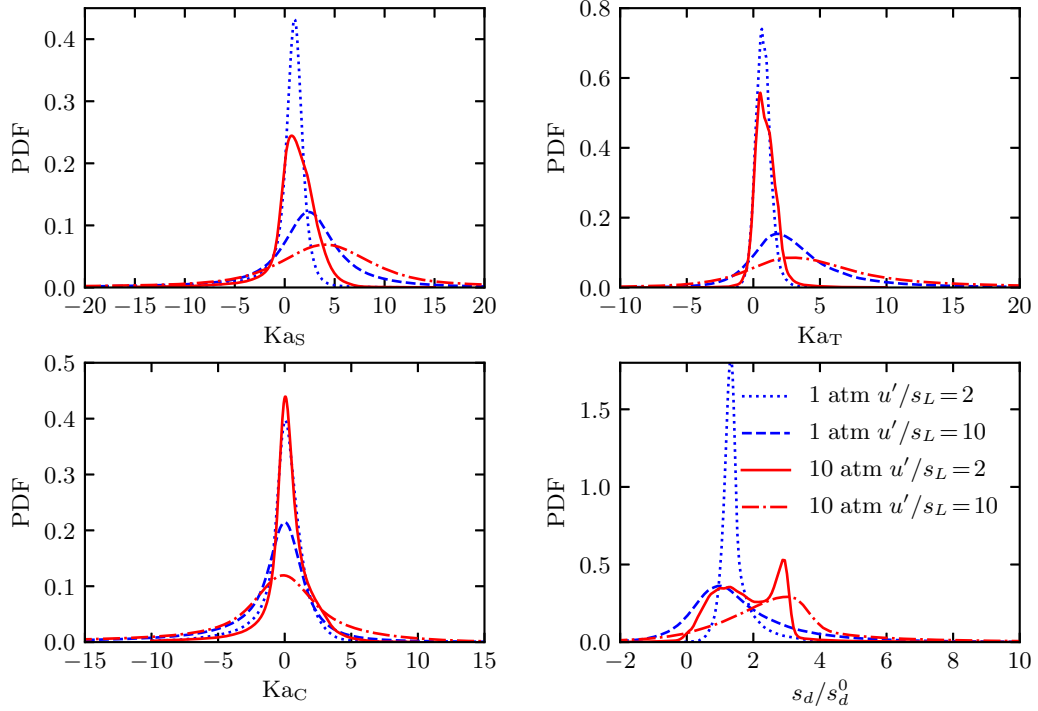


Figure 3: PDFs of the stretch-related Karlovitz numbers and local displacement speed at various pressures and turbulent intensities.

means, whereas PDFs of Ka_C keep roughly symmetric with the zero mean. Furthermore, PDFs of all the stretch-related Ka are widened with u'/s_L^0 [19] and pressure, and pressure effects on the PDFs become notable at high turbulence intensities, consistent with the different bending trends of s_T/s_L^0 in Fig. 1. It is clear that mean values of Ka_S and Ka_T increase with pressure for large u'/s_L^0 , whereas the increase is slight for small u'/s_L^0 . The PDFs in Fig. 3 indicate that Ka_T plays a dominant role in the positive stretching of turbulent flames, and Ka_C mainly contributes to broadening distributions of Ka_S .

In Fig. 3d, PDFs of s_d/s_d^0 show pressure effects on the local flame prop-

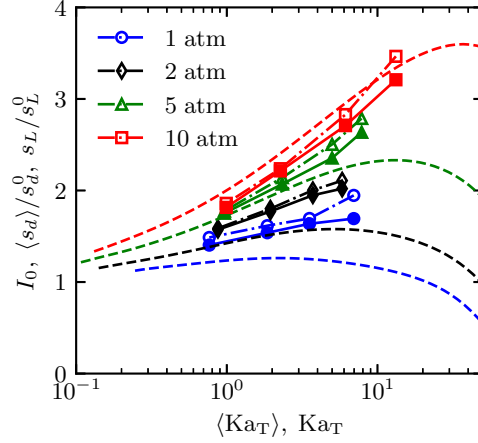


Figure 4: The stretch factor and its approximations in turbulent premixed flames and counterflow laminar flames (solid lines with solid symbols: I_0 ; dash-dotted lines with open symbols: $\langle s_d \rangle / s_d^0$; dashed lines: s_L / s_L^0). Both I_0 and $\langle s_d \rangle / s_d^0$ are plotted with respect to $\langle \text{Ka}_T \rangle$, and s_L / s_L^0 is plotted against Ka_T .

agation. At $p = 1$ atm, the distribution of s_d / s_d^0 is broadened with the turbulence intensity. At $p = 10$ atm, we observe two peaks in the PDF of s_d / s_d^0 for $u' / s_L^0 = 2$. The primary one is at $s_d / s_d^0 \approx 3$, and the secondary one is close to the peak at $p = 1$ atm around $s_d / s_d^0 = 1.1$. The two peaks are gradually merged with increasing u' / s_L^0 .

Figure 4 plots the stretch factor $I_0 = (s_T / s_L^0) / (A_T / A_L)$ in Eq. (2) and its approximation $\langle s_d \rangle / s_d^0$ in Eq. (3) with respect to $\langle \text{Ka}_T \rangle$ from combustion DNS, and the normalized laminar flame speed s_L / s_L^0 against Ka_T from laminar counterflow flames. The overall good agreement of $\langle s_d \rangle / s_d^0$ and I_0 in all the cases validates the approximation in Eq. (3).

In laminar counterflow flames, s_L / s_L^0 increases with stretching owing to the negative Markstein number (Ma) for the lean H_2 /air mixture. With the

increase of pressure, Ma decreases due to the higher activation energy and Zel'dovich number. Extensive studies of laminar flames [37] have shown that s_L/s_L^0 grows with Ka_T for weak and moderate stretch. Moreover, we observe that the growth of s_L/s_L^0 is generally enhanced by pressure with negative Ma . Similarly in all the turbulence cases, I_0 and $\langle s_d \rangle / s_d^0$ also grow with pressure and $\langle \text{Ka}_T \rangle$ which is proportional to the turbulence intensity. The consistency between $\langle s_d \rangle / s_d^0$ and s_L/s_L^0 inspires us to model I_0 in turbulent flames using laminar flame results.

3.3. Modeling of s_T at high pressures

We propose a predictive model for s_T at a range of pressures and turbulent intensities. Based on the validation of Eq. (5), the stretch factor and the flame area ratio are modeled separately.

For modeling the stretch factor, Fig. 4 suggests the consistency of I_0 and the response of s_L/s_L^0 to stretch of laminar flames, so we estimate I_0 using a lookup table \mathcal{F} formed by laminar flame data on s_L/s_L^0 versus Ka_T as

$$I_0 \left(\frac{u'}{s_L^0}, p \right) = \frac{s_L}{s_L^0} = \mathcal{F} \left(\sqrt{\frac{p}{20p_0}} \frac{u'}{s_L^0} \right), \quad (6)$$

where an empirical relation $\text{Ka}_T \approx \langle \text{Ka}_T \rangle \approx \sqrt{p/20p_0} (u'/s_L^0)$ with $p_0 = 1$ atm is employed for incorporating pressure effects.

For modeling the flame surface ratio, we extend the s_T model for standard pressure to high pressures. The original model is given in Eq. (3.30) in Ref. [18] with a detailed derivation based on Lagrangian statistics of propagating surfaces, and it has been validated using combustion DNS with various fuels at $p = 1$ atm.

We extend this model by including the influence of I_0 on A_T/A_L at high pressures as

$$\frac{A_T}{A_L} = \exp \left\{ T_\infty^* (\mathcal{A} + \mathcal{B} s_{L0}^0 I_0^2) \left[1 - \exp \left(- \frac{\mathcal{C} \text{Re}^{-1/4}}{T_\infty^* (\mathcal{A} + \mathcal{B} s_{L0}^0 I_0^2)} \frac{u'}{s_L^0 I_0} \right) \right] \right\}. \quad (7)$$

Here, universal model constants $\mathcal{A} = 0.317$, $\mathcal{B} = 0.033$, and $T_\infty^* = 5.5$ for turbulence effects are obtained from Lagrangian statistics of propagating or material surfaces in non-reacting HIT, and $s_{L0}^0 = s_L^0/s_{L,\text{ref}}$ is a dimensionless laminar flame speed normalized by a reference value $s_{L,\text{ref}} = 1$ m/s. These model constants are the same as those in the original model [18].

In the improved model in Eq. (7), the unstretched laminar flame speed in the original one is replaced by $s_L^0 I_0$ with flame stretch effects. The adapted model coefficient $\mathcal{C} = \mathcal{C}_0 I_0(u'/s_L^0 = 2, p)$ characterizes the combustion chemistry effect on the growth of s_T/s_L^0 in weak turbulence, where the constant $\mathcal{C}_0 = 2.5$ is suggested for hydrogen fuels in Ref. [18], and $I_0(u'/s_L^0 = 2, p)$ is used for recovering the linear growth of $s_T/s_L^0 = I_0 + \mathcal{C}_0(u'/s_L^0)$ in weak turbulence with $u'/s_L^0 < 2$ from Taylor expansions of Eq. (7). Furthermore, $\mathcal{A} + \mathcal{B} s_L$ in the original model approximates the growth rate of flame areas under the assumption of the constant local flame speed. Considering the effect of flame stretch on the mean and variance of local flame speed in Fig. 3d, s_L is approximated by $s_L^0 I_0^2$ here.

Finally, substituting Eqs. (6) and (7) and all the model coefficients into

Eq. (2) yields the s_T model including pressure effects as

$$\frac{s_T}{s_L^0} = \mathcal{F} \left(\sqrt{\frac{p}{20p_0}} \frac{u'}{s_L^0} \right) \times \exp \left\{ (1.742 + 0.182s_{L0}^0 \mathcal{F}^2) \left[1 - \exp \left(-\frac{2.5\mathcal{F}(\sqrt{p/(5p_0)}) \text{Re}^{-1/4} u'}{(1.742 + 0.182s_{L0}^0 \mathcal{F}^2) \mathcal{F} s_L^0} \right) \right] \right\}. \quad (8)$$

We remark that Eq. (8) only depends on given flame/flow parameters, universal model constants, and laminar flame data, so it is a predictive model of s_T for turbulent premixed flames.

The s_T model in Eq. (8) is validated by DNS results in Fig. 5. In general, the present model shows quantitatively good predictions on important phenomena in turbulent premixed flames at a broad range of turbulent intensities and pressures. Around 1 atm, the model predicts the bending curve at moderate and large u'/s_L^0 . As the pressure increases, our model well captures the rise of s_T/s_L^0 and the suppression of bending by accounting for pressure effects.

4. Conclusions

We elucidate the pressure effects on s_T and propose a predictive s_T model for turbulent premixed flames. First we carried out a series of DNS for lean H₂/air turbulent premixed flames in HIT at $p = 1$ to 10 atm and $u'/s_L^0 = 2$ to 20. The DNS results show bending curves of s_T/s_L^0 with respect to u'/s_L^0 . In particular, s_T/s_L^0 for the same u'/s_L^0 increases with pressure, and the bending is suppressed at elevated pressures.

We further demonstrate both the turbulent flame area and stretch factor contribute to the rise of s_T/s_L^0 at elevated pressures for lean H₂/air flames.

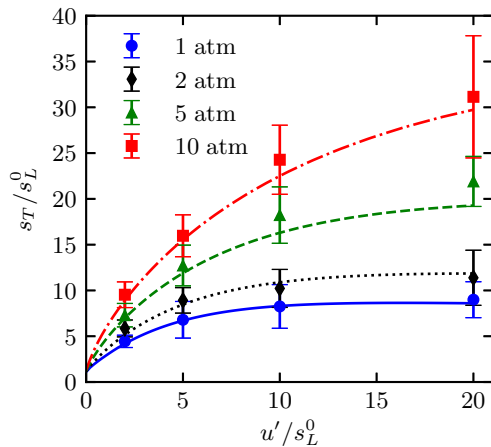


Figure 5: Comparison of s_T calculated from combustion DNS (symbols with error bars for one standard deviation) and the proposed model Eq. (8) (lines) at various pressures.

The turbulent flame area has similar bending phenomena at various pressures. The increased flame stretch sensitivity with pressure leads to the growth of I_0 at the high turbulence intensity and pressure. In addition, large I_0 enhances the growth of A_T via the increase of the local flame speed.

From the analysis on DNS results, we extend the s_T model for standard pressure [18] to high pressures via modeled I_0 . We find that the variation of I_0 with $\langle Ka_T \rangle$ in turbulent premixed flames is similar to that of the laminar flame speed with flame stretch, so a lookup table for modeling I_0 is employed using laminar flame data at different pressures. The flame area model based on Lagrangian statistics of propagating surfaces is extended by incorporating I_0 for the increased mean and variance of the local flame speed at high pressures.

Finally, we estimate s_T/s_L^0 as the product of modeled I_0 and A_T/A_L . This predictive s_T model only depends on given flame and flow parameters, uni-

versal model constants, and laminar flame data. The comparison between model predictions and DNS results shows overall good agreement, including the bending trends, in all the DNS cases at a broad range of turbulent intensities and pressures.

It is noted that the present study only considers the unburnt mixture with negative Markstein numbers in HIT, and the unity ratio of the turbulence length scale and flame thickness. In the future work, s_T for different fuels and flame geometries at elevated pressures will be investigated with further validations of the proposed s_T model.

Acknowledgments

We gratefully acknowledge Caltech, the University of Colorado at Boulder and Stanford University for licensing the NGA code used in this work. This work has been supported in part by the National Natural Science Foundation of China (Grant Nos. 91541204, 11925201, and 91841302).

References

- [1] N. Peters, Turbulent Combustion, Cambridge University Press, 2000.
- [2] A. Lipatnikov, J. Chomiak, Turbulent flame speed and thickness: Phenomenology, evaluation, and application in multi-dimensional simulations, Prog. Energy Combust. Sci. 28 (2002) 1 – 74.
- [3] J. F. Driscoll, Turbulent premixed combustion: Flamelet structure and its effect on turbulent burning velocities, Prog. Energy Combust. Sci. 34 (2008) 91 – 134.

- [4] S. Daniele, P. Jansohn, J. Mantzaras, K. Boulouchos, Turbulent flame speed for syngas at gas turbine relevant conditions, *Proc. Combust. Inst.* 33 (2011) 2937 – 2944.
- [5] H. Kobayashi, Y. Otawara, J. Wang, F. Matsuno, Y. Ogami, M. Okuyama, T. Kudo, S. Kadowaki, Turbulent premixed flame characteristics of a CO/H₂/O₂ mixture highly diluted with CO₂ in a high-pressure environment, *Proc. Combust. Inst.* 34 (2013) 1437 – 1445.
- [6] D. Bradley, M. Lawes, K. Liu, M. Mansour, Measurements and correlations of turbulent burning velocities over wide ranges of fuels and elevated pressures, *Proc. Combust. Inst.* 34 (2013) 1519 – 1526.
- [7] P. Venkateswaran, A. Marshall, J. Seitzman, T. Lieuwen, Scaling turbulent flame speeds of negative Markstein length fuel blends using leading points concepts, *Combust. Flame* 162 (2015) 375 – 387.
- [8] R. Fragner, F. Halter, N. Mazellier, C. Chauveau, I. Gökalp, Investigation of pressure effects on the small scale wrinkling of turbulent premixed Bunsen flames, *Proc. Combust. Inst.* 35 (2015) 1527 – 1535.
- [9] J. Wang, S. Yu, M. Zhang, W. Jin, Z. Huang, S. Chen, H. Kobayashi, Burning velocity and statistical flame front structure of turbulent premixed flames at high pressure up to 1.0MPa, *Exp. Thermal Fluid Sci.* 68 (2015) 196 – 204.
- [10] M. T. Nguyen, D. W. Yu, S. S. Shy, General correlations of high pressure turbulent burning velocities with the consideration of Lewis number effect, *Proc. Combust. Inst.* 37 (2019) 2391 – 2398.

- [11] H. Kobayashi, T. Kawahata, K. Seyama, T. Fujimari, J.-S. Kim, Relationship between the smallest scale of flame wrinkles and turbulence characteristics of high-pressure, high-temperature turbulent premixed flames, *Proc. Combust. Inst.* 29 (2002) 1793 – 1800.
- [12] H. G. Im, P. G. Arias, S. Chaudhuri, H. A. Uranakara, Direct numerical simulations of statistically stationary turbulent premixed flames, *Combust. Sci. Technol.* 188 (2016) 1182–1198.
- [13] M. S. Day, J. B. Bell, P.-T. Bremer, V. Pascucci, V. Beckner, M. Lijewski, Turbulence effects on cellular burning structures in lean premixed hydrogen flames, *Combust. Flame* 156 (2009) 1035 – 1045.
- [14] A. J. Aspden, J. B. Bell, M. S. Day, F. N. Egolfopoulos, Turbulence–flame interactions in lean premixed dodecane flames, *Proc. Combust. Inst.* 36 (2017) 2005 – 2016.
- [15] H. A. Uranakara, S. Chaudhuri, H. L. Dave, P. G. Arias, H. G. Im, A flame particle tracking analysis of turbulence–chemistry interaction in hydrogen–air premixed flames, *Combust. Flame* 163 (2016) 220 – 240.
- [16] J. H. Chen, H. G. Im, Correlation of flame speed with stretch in turbulent premixed methane/air flames, *Proc. Combust. Inst.* 27 (1998) 819 – 826.
- [17] G. Nivarti, S. Cant, Direct numerical simulation of the bending effect in turbulent premixed flames, *Proc. Combust. Inst.* 36 (2017) 1903 – 1910.
- [18] J. You, Y. Yang, Modelling of the turbulent burning velocity based

- on Lagrangian statistics of propagating surfaces, submitted to *J. Fluid Mech.* (2019). [arXiv:1911.00220](https://arxiv.org/abs/1911.00220).
- [19] B. Savard, S. Lapointe, A. Teodorczyk, Numerical investigation of the effect of pressure on heat release rate in iso-octane premixed turbulent flames under conditions relevant to SI engines, *Proc. Combust. Inst.* 36 (2017) 3543 – 3549.
- [20] Z. Wang, V. Magi, J. Abraham, Turbulent flame speed dependencies in lean methane-air mixtures under engine relevant conditions, *Combust. Flame* 180 (2017) 53 – 62.
- [21] X. Wang, T. Jin, Y. Xie, K. H. Luo, Pressure effects on flame structures and chemical pathways for lean premixed turbulent H₂/air flames: Three-dimensional DNS studies, *Fuel* 215 (2018) 320 – 329.
- [22] B. Savard, H. Wang, A. Wehrfritz, E. R. Hawkes, Direct numerical simulations of rich premixed turbulent n-dodecane/air flames at diesel engine conditions, *Proc. Combust. Inst.* 37 (2019) 4655 – 4662.
- [23] P. Venkateswaran, A. Marshall, D. H. Shin, D. Noble, J. Seitzman, T. Lieuwen, Measurements and analysis of turbulent consumption speeds of H₂/CO mixtures, *Combust. Flame* 158 (2011) 1602 – 1614.
- [24] L. Vervisch, E. Bidaux, K. N. C. Bray, W. Kollmann, Surface density function in premixed turbulent combustion modeling, similarities between probability density function and flame surface approaches, *Phys. Fluids* 7 (1995) 2496–2503.

- [25] S. S. Girimaji, S. B. Pope, Propagating surfaces in isotropic turbulence, *J. Fluid Mech.* 234 (1992) 247–277.
- [26] T. Zheng, J. You, Y. Yang, Principal curvatures and area ratio of propagating surfaces in isotropic turbulence, *Phys. Rev. Fluids* 2 (2017) 103201.
- [27] O. Desjardins, G. Blanquart, G. Balarac, H. Pitsch, High order conservative finite difference scheme for variable density low Mach number turbulent flows, *J. Comput. Phys.* 227 (2008) 7125 – 7159.
- [28] Z. Ren, S. B. Pope, Second-order splitting schemes for a class of reactive systems, *J. Comput. Phys.* 227 (2008) 8165–8176.
- [29] C. D. Pierce, Progress-variable approach for large-eddy simulation of turbulent combustion, Ph.D. thesis, Stanford University, Stanford, CA, USA (2001).
- [30] M. Herrmann, G. Blanquart, V. Raman, Flux corrected finite volume scheme for preserving scalar boundedness in reacting large-eddy simulations, *AIAA J.* 44 (2006) 2879–2886.
- [31] P. N. Brown, G. D. Byrne, A. C. Hindmarsh, VODE: A variable-coefficient ODE solver, *SIAM J. Sci. Stat. Comput.* 10 (1989) 1038–1051.
- [32] J. Li, Z. Zhao, A. Kazakov, F. L. Dryer, An updated comprehensive kinetic model of hydrogen combustion, *Int. J. Chem. Kinet.* 36 (2004) 556–575.

- [33] N. Burali, S. Lapointe, B. Bobbitt, G. Blanquart, Y. Xuan, Assessment of the constant non-unity Lewis number assumption in chemically-reacting flows, *Combust. Theory Model.* 20 (2016) 632–657.
- [34] S. B. Pope, *Turbulent Flows*, Cambridge University Press, 2000.
- [35] P. L. Carroll, G. Blanquart, A proposed modification to Lundgren’s physical space velocity forcing method for isotropic turbulence, *Phys. Fluids* 25 (2013) 105114.
- [36] K. N. C. Bray, R. S. Cant, Some applications of Kolmogorov’s turbulence research in the field of combustion, *Proc. R. Soc. London A* 434 (1991) 217–240.
- [37] C. K. Law, *Combustion Physics*, Cambridge University Press, 2006.